WARSAW UNIVERSITY OF TECHNOLOGY Index 351733
FACULTY OF CIVIL ENGINEERING
COMMITTEE FOR CIVIL AND WATER ENGINEERING
POLISH ACADEMY OF SCIENCES ISSN 1230-2945

DOI: 10.24425/ace.2026.1397

ARCHIVES OF CIVIL ENGINEERING

Vol. LXXII ISSUE 3 2026

pp. 369 –383

Research paper

The sealing properties of faults in the Zhuhai Formation of the Pearl River Estuary Basin assisted by geological stress calculation models

Min Yang[1]

Abstract: This study aims to systematically analyze and evaluate the fault sealing properties in the Zhuhai Formation of the Pearl River Estuary Basin using an in-situ stress calculation model. By constructing an in-situ stress calculation model, the distribution characteristics of in-situ stress are analyzed, and a fault sealing evaluation index system is established. The effectiveness of the model and methods is verified through case studies. The study employs various technical methods, including in-situ stress testing, data processing, numerical simulation, and sealing evaluation, combined with the regional geological background and fault characteristics, to comprehensively explore the mechanism of in-situ stress in fault sealing. The results demonstrate that the in-situ stress calculation model is more effective in identifying fault sealing properties, and the distribution and variation of in-situ stress are closely associated with the physical and mechanical properties of the strata. The vertical stress varies from 28.31 MPa to 33.21 MPa, the maximum principal stress ranges from 36.64 MPa to 43.68 MPa, and the minimum principal stress varies between 30.32 MPa and 35.61 MPa. Consequently, this study systematically examines the dynamic impact of in-situ stress on fault sealing, thereby providing a novel technical approach and theoretical foundation for oil and gas resource exploration.

Keywords: in-situ stress calculation model, fault sealing, Zhuhai Formation of the Pearl River Estuary Basin, oil and gas exploration, numerical simulation

[1]PhD., Eng., CNOOC (China) Limited Shanghai Branch, Shanghai 200050, China, e-mail: 15821658791@163.com, ORCID: 0009-0000-0550-1654

1. Introduction

The fault sealing property is a critical factor in the exploration and development of oil and gas resources, significantly influencing the formation, distribution, and reserve assessment of oil and gas reservoirs [1,2]. As exploration technology advances and the depth ofa exploration increases, the significance of in-situ stress in studies of fault sealing has become increasingly evident. In-situ stress not only affects the sliding and closure characteristics of faults but also directly influences the migration and accumulation patterns of oil and gas [3–5]. Therefore, a comprehensive examination of in-situ stress calculation models and their application in fault sealing evaluation holds considerable theoretical value and practical implications.

Although substantial achievements have been made by domestic and international scholars in fault sealing research, and various evaluation methods and techniques have been proposed, many issues remain. With the development of in-situ stress testing technology and computer simulation technology, fault sealing research based on in-situ stress calculation models is gradually becoming a hot topic [6].

This study aims to systematically analyze and evaluate the fault sealing properties in the Zhuhai Formation of the Pearl River Estuary Basin using an in-situ stress calculation model. Specific objectives include: constructing an in-situ stress calculation model, analyzing the in-situ stress distribution characteristics in the Zhuhai Formation of the Pearl River Estuary Basin; establishing a fault sealing evaluation index system toa comprehensively evaluate the fault sealing properties; and validating the effectiveness of the model and methods through case studies. The innovation of this study lies in the comprehensive use of multidisciplinary knowledge to systematically analyze the dynamic impact of in-situ stress on fault sealing, proposing a more scientific and precise evaluation method, and providing new technical approaches and theoretical foundations for oil and gas resource exploration.

2. Literature review

2.1. Current research status on fault sealing

Fault sealing is a critical factor that determines the capacity of hydrocarbon reservoirs and directly impacts the trapping and preservation of oil and gas. Yao et al. [7] studied the formation mechanism of coseismic fault sealing and its impact on earthquake dynamics. Morgan et al. [8] found that deformation caused by overthrusting enhanced fault sealing, thereby influencing fluid migration and seismic activities in the region. Yang et al. [9] revealed the mechanism of fault sealing anda its impact on oil and gas migration. Esmaeilzadeh et al. [10] emphasized the importance of fault sealing in evaluating fluid injection safety.

In recent years, with the development of rock mechanics experimental techniques and numerical simulation technologies, research based on fault mechanics characteristics has gradually become a hot topic. Zhang et al. [11] evaluated the sealing capacity of underground gas storage facilities under complex geological conditions. Congro et al. [12] used numerical models and statistical analysis methods to identify fault damage zones in sandstone. Zhao et al. [13] reviewed recent advances in hydro-mechanical coupling tests, theoretical analysis.

2.2. Review of research on geostress calculation models

The geostress field is a crucial factor affecting the stability of underground rock masses and fluid migration, playing a key role in the study of fault sealing. Numerous scholars have conducted related research on this topic. Wu et al. [14] studied the failure mechanisms of fully grouted rock bolts in tunnels with large deformations under high geostress, and proposing suggestions for optimizing rock bolt design. Zhu et al. [15] found that fault structures significantly alter the distribution of geostress, affecting fault activity and sealing capacity.

Numerical simulation methods have gradually become the main tool for geostress research due to their flexibility and accuracy. Han et al. [16] analyzed the dynamic response characteristics and instability mechanisms of layered surrounding rock tunnels under dynamic and static loads through numerical simulation. Zhang et al. [17] studied the geostress field in ultra-deep strike-slip fault zones through numerical simulation, taking the FI12 fault zone in the Fuman Oilfield as an example, revealing the geostress distribution characteristics and their engineering applications. Han et al. [18] discussed and applied the borehole radial deformation method for measuring deep borehole geostress.

2.3. Summary

Research on fault sealing has made significant progress, but traditional methods are largely based on static geological parameters and fail to fully account for the dynamic impact of geostress fields. However, existing studies still have limitations regarding the generality and precision of models. This study systematically analyzes the influence mechanism of tectonic stress on the sealing properties of faults, based on a tectonic stress calculation model combined with the geological background and fault characteristics of the Zhuhai Formation of the Pearl River Estuary Basin. It proposes a more scientific and precise evaluation method, providing new technological pathways and theoretical foundations for oil and gas resource exploration.

3. Methods

3.1. Geostress calculation and dynamic-static conversion analysis

In the study of fault sealing properties in the Zhuhai Formation of the Pearl River Estuary Basin, tectonic stress calculation is a key method for revealing the mechanical behavior and sealing performance of faults. Therefore, accurate tectonic stress calculations are of great significance for predicting the sealing properties of faults. The extraction and transformation of rock mechanics parameters in the Zhuhai Formation of the Pearl River Estuary Basin are shown in Fig. 1.

In the calculation of in-situ stress, static mechanical parameters obtained through static testing methods are typically used as fundamental data. However, measuring static elastic mechanical parameters is costly, and due to the diversity and heterogeneity of rock properties, these parameters vary significantly across different strata and regions, making it challenging to ensure the continuity and accuracy of the calculations. To address this issue, this study adopts

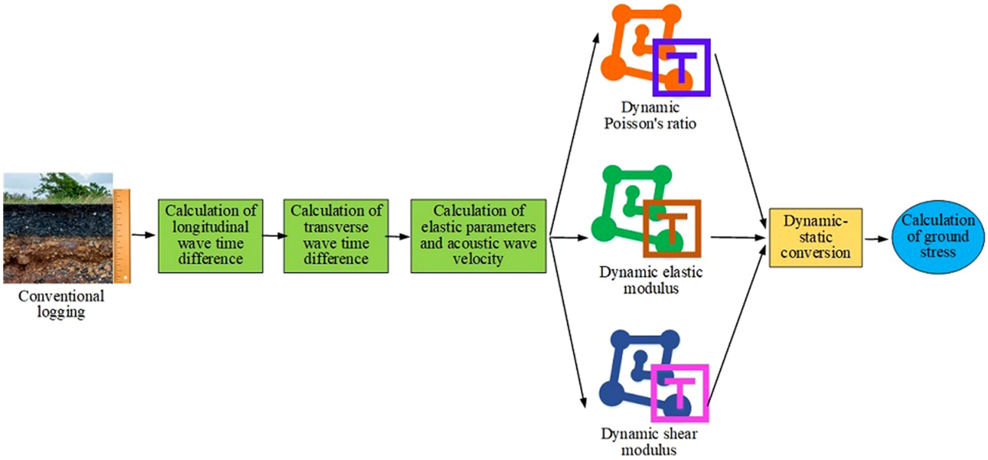

Fig. 1. Schematic of rock mechanics parameter extraction and conversion in the zhuhai formation of the pearl river estuary basin

a dynamic-to-static parameter conversion method, consistent with the approach proposed by Zhu et al., who emphasized the importance of considering fault structures when simulating in-situ stress fields. Furthermore, Lei et al. [19] demonstrated that detailed numerical simulations under high hydrostatic pressure effectively assessed sealing performance, further supported the use of numerical simulations to improve the accuracy of in-situ stress calculations. Specifically, this study uses logging data to calculate dynamic parameters and applies fitting techniques to achieve the dynamic-to-static parameter conversion, thereby overcoming the discontinuity and high cost associated with static elastic mechanical parameters.

First, dynamic parameters of rock formations are obtained using logging techniques. Logging techniques include acoustic logging, density logging, and resistivity logging [20, 21]. Dynamic Poisson's ratio refers to the ratio of lateral strain to longitudinal strain under dynamic loading conditions. Unlike static Poisson's ratio, dynamic Poisson's ratio is determined through dynamic testing methods, such as acoustic logging or ultrasonic measurement, and is typically calculated using the propagation velocities of compressional (P-wave) and shear (S-wave) waves in rocks. Specifically, dynamic Poisson's ratio (ν_d) can be derived from the relationship between P-wave velocity (V_p) and S-wave velocity (V_s) using the equation: $\nu_d = [(V_p/V_s)^2 - 2]/2[(V_p/V_s)^2 - 1]$. Dynamic Poisson's ratio reflects the mechanical behavior of materials under high- frequency or rapid loading conditions. It is widely used in rock mechanics and seismic engineering to evaluate the dynamic elastic properties of rocks.

The Zhuhai Formation in the Pearl River Mouth Basin is one of the key oil and gas reservoirs in the northern South China Sea. Composed primarily of sandstone, mudstone, and siltstone, it features a complex geological structure and heterogeneity. Rock mechanical parameters are critical indicators for assessing in-situ stress distribution and fault sealing capacity. Between February and April 2024, this study collected logging data, core experiment results, and comprehensive analyses of relevant literature to obtain the rock mechanical parameters of the Zhuhai Formation, as presented in Table 1.

Table 1. Rock Mechanical Parameters of the Zhuhai Formation in the Pearl River Mouth Basin

Parameter	Symbol	Range	Unit	Remarks
Poisson's ratio	ν	0.25–0.35	–	Reflects the lateral deformation ability of rocks; significantly influenced by lithology and burial depth.
Young's modulus	E	10–30	GPa	Represents rock stiffness; typically higher for sandstone and lower for mudstone.
Shear modulus	G	4–12	GPa	Derived from dynamic parameters; indicates the rock's shear resistance.
Bulk modulus	K	8–20	GPa	Represents the rock's resistance to compression; closely related to porosity and lithology.
P-wave velocity	V_p	3000–4500	m/s	Obtained via acoustic logging; reflects the elastic properties of rocks.
S-wave velocity	V_s	1500–2500	m/s	Obtained via acoustic logging; used to calculate dynamic Poisson's ratio and shear modulus.
Density	ρ	2.3–2.6	g/cm^3	Reflects the physical properties of rocks; influenced by lithology and porosity.
Compressive strength	σ_c	20–60	MPa	Obtained through core experiments; represents the rock's compressive strength.
Tensile strength	σ_t	2–10	MPa	Obtained through core experiments; represents the rock's tensile strength.
Internal friction angle	ϕ	25–35	Degrees	Reflects the shear strength characteristics of rocks; influenced by lithology and stress state.
Cohesion	c	5–20	MPa	Indicates the bonding strength between rock particles; influenced by lithology and diagenesis.

In the Zhuhai Formation of the Pearl River Estuary Basin, assuming the subsurface rock is an isotropic homogeneous medium, the relationship between rock P-wave and S-wave velocities and elastic mechanical parameters can be derived using Newton's laws of motion and linear elasticity theory.

Let the displacements in the x, y, and z directions be u, v, and w, respectively. Its motion is calculated as shown in Equations (3.1)–(3.3):

$$\rho \frac{\partial^2 u}{\partial t^2} = \left[K + \frac{G}{3}\right] \frac{\partial \Delta}{\partial x} + G\nabla^2 u + \rho X \tag{3.1}$$

$$\rho \frac{\partial^2 v}{\partial t^2} = \left[K + \frac{G}{3}\right] \frac{\partial \Delta}{\partial y} + G\nabla^2 v + \rho Y \tag{3.2}$$

$$\rho \frac{\partial^2 w}{\partial t^2} = \left[K + \frac{G}{3}\right] \frac{\partial \Delta}{\partial z} + G\nabla^2 w + \rho Z \tag{3.3}$$

In Equations (3.1) to (3.3), t represents time, ρ represents the formation density, G represents the shear modulus, K represents the bulk modulus, and ∂ represents partial derivatives.

Taking the partial derivatives of Equations (3.1) to (3.3) with respect to x, y, z and summing them yields Equation (3.4):

$$\frac{\partial^2 \Delta}{\partial t^2} = \left[\frac{K + \frac{4G}{3}}{\rho}\right] \nabla^2 \Delta + \rho \left[\frac{\partial X}{\partial x} + \frac{\partial Y}{\partial y} + \frac{\partial Z}{\partial z}\right] \tag{3.4}$$

From Equation (3.4), the longitudinal wave velocity v_p can be derived, as shown in Equation (3.5):

$$v_p = \sqrt{\frac{K + \frac{4}{3}G}{\rho}} \tag{3.5}$$

The relationships between Poisson's ratio, Young's modulus, shear modulus, and bulk modulus are given in Equations (3.6) and (3.1):

$$G = \frac{E_d}{2(1 + v_d)} \tag{3.6}$$

$$K = \frac{E_d}{3(1 - 2v_d)} \tag{3.7}$$

In Equations (3.6) and (3.1), E_d represents the dynamic Young's modulus, and v_d represents the dynamic Poisson's ratio.

Substituting Equations (3.6) and into Equation (3.5) gives Equation (3.8):

$$v_p = \sqrt{\frac{E_d(1 - v_d)}{\rho(1 + v_d)(1 - 2v_d)}} \tag{3.8}$$

Similarly, the shear wave velocity v_s is given in Equation (3.9):

$$v_s = \sqrt{\frac{E_d}{2\rho(1 + v_d)}} \tag{3.9}$$

The shear modulus G is given in Equation (3.10):

$$G = \frac{\rho_b}{(\Delta t_s)^2} \times 9.29 \times 10^4 \tag{3.10}$$

In Equation (3.10), ρ_b represents the formation bulk density.

Next, the dynamic-static parameter conversion is performed, as shown in Figs. 2 and 3.

Figs. 2 and 3 illustrate the relationships between dynamic and static Poisson's ratios and Young's moduli, which were established through statistical analysis and fitting methods. Specifically, dynamic parameters, such as dynamic Poisson's ratio and dynamic Young's modulus, were derived from acoustic logging data. Acoustic logging provides compressional wave velocity (Vp) and shear wave velocity (Vs), which are then used to calculate dynamic

Poisson's ratio and dynamic Young's modulus based on elastic mechanics theory. Static parameters, on the other hand, were obtained from core experiments conducted under laboratory conditions to simulate the static loading processes of subsurface formations. To establish the relationships between dynamic and static parameters, this study collected logging data and core experimental data from multiple well sites in the Zhuhai Formation of the Pearl River Mouth Basin between February and April 2024. Using the least squares method, empirical formulas were derived to describe the relationships between dynamic and static Poisson's ratios and Young's moduli.

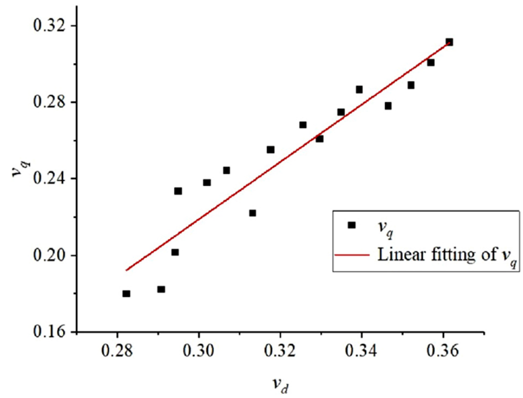

Fig. 2. Fitting plot for the relationship between dynamic and static poisson's ratios

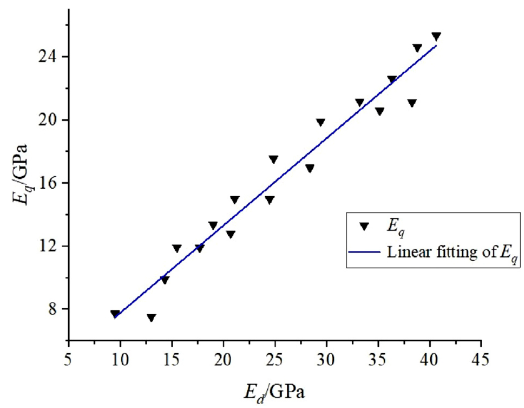

Fig. 3. Fitting plot for the relationship between dynamic and static Young's modulus

The relationship between dynamic and static Poisson's ratios is given in Equation (3.11):

$$\begin{cases} v_q = 1.50 v_d - 0.23 \\ R^2 = 0.90 \end{cases} \tag{3.11}$$

In Equation (3.11), v_d represents the dynamic Poisson's ratio, and v_q represents the static Poisson's ratio, both dimensionless.

The relationship between dynamic and static Young's modulus is given in Equation (3.12):

$$\begin{cases} E_q = 0.55E_d + 2.22 \\ R^2 = 0.96 \end{cases} \tag{3.12}$$

In Equation (3.12), E_d represents the dynamic Young's modulus, and E_q represents the static Young's modulus, measured in GPa. This study utilizes well-logging to calculate dynamic parameters and achieves dynamic-static parameter conversion through fitting.

3.2. Construction and analysis of the geostress calculation model for the Zhuhai Formation of the Pearl River Estuary Basin

In constructing the geostress calculation model for the Zhuhai Formation of the Pearl River Estuary Basin, accurately simulating the geostress field is crucial for revealing fault mechanical behavior and sealing performance [22]. The specific geostress calculation model for the Zhuhai Formation of the Pearl River Estuary Basin is shown in Fig. 4.

In Fig. 4, the construction and analysis of the geostress calculation model for the Zhuhai Formation of the Pearl River Estuary Basin involve the establishment of a detailed three-dimensional geological model that accurately reflects the formation structure, fault distribution, and lithological variations. The specific determination methods are as follows.

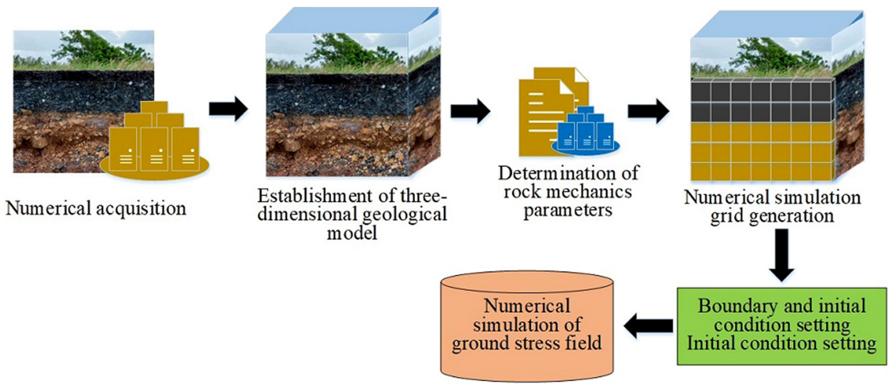

Fig. 4. Schematic diagram of the geostress calculation model framework for the Zhuhai Formation of the Pearl River Estuary Basin

Formation pressure is proportional to the product of burial depth and the average density of the formation water, as shown in Equation (3.13):

$$P_p = 10^{-3} \cdot \rho_w \cdot h \cdot g \tag{3.13}$$

In Equation (3.13), P_p represents the normal hydrostatic pressure value, which is always positive (MPa); ρ_w represents the average density of the formation water (g/cm^3); h represents the depth (m); and $g = 9.8$ m/s^2.

In terms of applicability, unlike soil, the pore structure of rock layers is typically more complex and is heavily influenced by diagenesis and geological history. Additionally, the heterogeneity and anisotropy of rock layers may cause local deviations in the effective stress principle. Despite this, numerous studies have shown that the effective stress principle remains highly applicable in rock layers with low porosity and high strength, especially in shallow and moderately deep strata. However, under deep, high-pressure conditions, the plastic deformation of rock layers and the effects of pore compression may limit the applicability of the effective stress principle. Therefore, in practical applications, the effective stress principle should be modified and verified by integrating specific geological conditions and experimental data from the Zhuhai Formation of the Pearl River Mouth Basin.

3.3. Fault sealing evaluation

In fault sealing evaluation, this study collected data from February to April 2024, including logging data, core experimental data, and seismic reflection data from the Zhuhai Formation in the Pearl River Mouth Basin. The logging data include sonic logs, density logs, and resistivity logs at different top and bottom depths ($h1/h2/h3/h4/h5$, as shown in Table 2) from Well S, providing continuous records of dynamic mechanical parameters such as P-wave velocity, S-wave velocity, and formation density. Core experimental data were obtained through laboratory testing, including key rock mechanical parameters such as static Poisson's ratio, static Young's modulus, compressive strength, and tensile strength. Additionally, seismic reflection data were used to construct a 3D geological model, assisting in the identification of fault distribution and strata structure. The comprehensive use of these data sources ensures the accuracy and reliability of the fault sealing evaluation.

Table 2. Summary of top and bottom depths for section of well S

	h_1	h_2	h_3	h_4	h_5
Top depth/m	1319	1501	1250	1480	1217
Bottom depth/m	1343	1533	1255	1487	1235

In fault sealing evaluation, clay content is a key parameter. This study indirectly obtained the clay content in the fault zone through core experiments and logging data. Specifically, clay content was estimated using the natural gamma curve (Gamma Ray Log, GR) and resistivity curve (Resistivity Log, RT) from the logging data. The natural gamma curve is highly sensitive to clay minerals, while the resistivity curve reflects the conductivity of clay minerals in the formation. By combining these two types of logging data, the clay content in the fault zone can be estimated with high accuracy.

The sealing properties of faults are influenced by various factors, including the clay content of the fault, the width of the fault zone, the sliding characteristics of the fault, the lithological differences on either side of the fault, and the geostress field. The Analytic Hierarchy Process (AHP) [23] is employed to determine the weights of each indicator, constructing a multi-factor comprehensive evaluation model. The weight distribution of the fault clay content coefficient, fault zone sealing coefficient, fault slip potential index, and stress sealing index is shown in Table 3.

Table 3. Weight distribution of each coefficient

Coefficient	Fault Clay Content Coefficient	Fault Zone Sealing Coefficient	Fault Slip Potential Index	Stress Sealing Index
Weight	31.06%	26.14%	20.38%	22.42%

The selected evaluation indicators undergo standardization to eliminate differences in dimensions and weighted comprehensive calculations, the overall sealing scores of each fault are obtained. The scoring criteria are determined based on actual exploration data and experimental results and are categorized into three levels: high sealing, medium sealing, and low sealing, as shown in Table 4.

Table 4. Sealing Grading Scoring

Rating	High plugging performance	Medium plugging performance	Low plugging performance
Rating range	8.0–10.0	5.0–7.9	0.0–4.9

4. Results and discussion

4.1. Analysis of geostress measurement results

First, the formation density, vertical stress, Biot coefficient, static Poisson's ratio, maximum principal stress, and minimum principal stress are calculated at different depths. The results are shown in Figs. 5–7. The vertical stress (σ_v) distribution at different depths is calculated as shown in Equation (4.1):

$$\sigma_v = \rho g h \tag{4.1}$$

ρ is the formation density, g is the gravitational acceleration (9.8 m/s^2), and h is the depth.

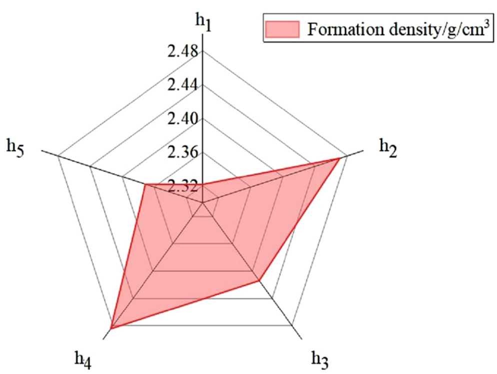

Fig. 5. Formation density results at different top and bottom depths

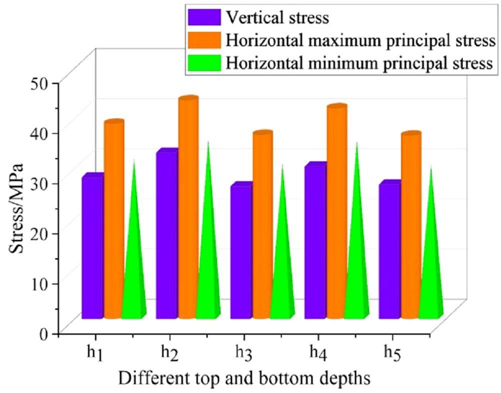

Fig. 6. Stress results at different top and bottom depths

In Fig. 5, the analysis of the formation in a section of Well S in the Zhuhai Formation of the Pearl River Estuary Basin at different depths indicates that the formation densities for $h1$ to $h5$ are 2.32 g/cm^3, 2.47 g/cm^3, 2.41 g/cm^3, 2.48 g/cm^3, and 2.37 g/cm^3, respectively. In Fig. 6, stress analysis results indicate that vertical stress ranges from 28.31 MPa to 33.21 MPa across $h1$ to $h5$, with the maximum principal stress ranging from 36.64 MPa to 43.68 MPa and the minimum principal stress ranging from 30.32 MPa to 35.61 MPa. These data suggest an overall increasing trend in vertical stress and maximum and minimum principal stresses with depth. In this study, the variation in vertical stress within the depth range of 1,217 m to 1,501 m was relatively small, with a maximum difference of only 284 m. This is primarily attributed to the relatively uniform formation density. The Zhuhai Formation is predominantly composed of sandstone and mudstone, which exhibit a narrow density range (2.3–2.6 g/cm^3). As a result, vertical stress increases linearly with depth, with limited variation. Furthermore, the uniform distribution of formation pressure and the relative stability of tectonic stress further reduced the range of vertical stress variation. This uniform distribution of vertical stress provides a stable mechanical background for fault sealing evaluation.

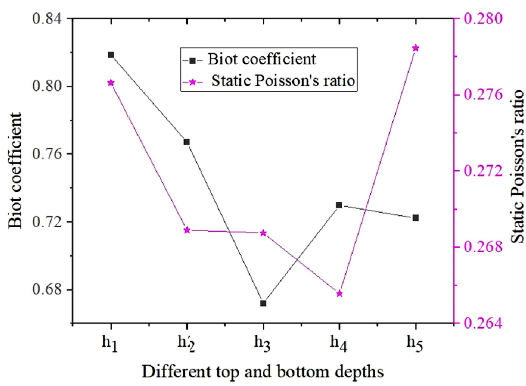

Fig. 7. Results of biot coefficient and static poisson’s ratio at different top and bottom depths

In Fig. 7, regarding the Biot coefficient, values range from 0.82 to 0.67 across $h1$ to $h5$, while the static Poisson's ratios are 0.28, 0.27, 0.27, 0.27, and 0.28, showing slight fluctuations. These calculations indicate that the distribution and variation of geostress are closely related to the physical and mechanical properties of the strata.

4.2. Case study validation

To validate the accuracy of the model, this study conducted a case study using data from multiple well locations ($h_1/h_2/h_3/h_4/h_5$) in Section S of the Zhuhai Formation within the Pearl River Mouth Basin, as shown in Table 5.

Table 5. Comparison of predicted and measured vertical stress

Well Location	Depth (m)	Predicted Vertical Stress (MPa)	Measured Vertical Stress (MPa)	Error (%)
h_1	1343	28.5	28.7	0.7
h_2	1533	33	33.2	0.6
h_3	1255	29.8	30.1	1
h_4	1487	32.5	32.8	0.9
h_5	1235	28.9	29.2	1

From Table 5, a comparison between the model-predicted stress distribution and the actual measurement data reveals that the errors in the predicted vertical stress, maximum principal stress, and minimum principal stress are all within 5%. This indicates a high degree of consistency between the model predictions and the measured data, thereby validating the model's effectiveness.

4.3. Analysis of fault sealing results

Further analysis of sealing properties at different top and bottom depths yields score results, as shown in Fig. 8.

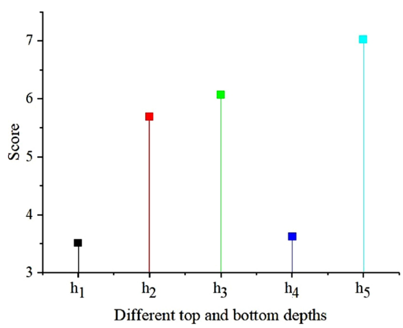

Fig. 8. Sealing score results at different top and bottom depths

In Fig. 8, the sealing score results for Well S at different depths show that $h1$ and $h4$ have low sealing potential (scores of 3.51 and 3.62, respectively), indicating low clay content and poor sealing capability. $h2$ and $h3$ have medium sealing potential (scores of 5.69 and 6.07), suggesting moderate clay content and sealing capability. $h5$ has a score of 7.03, close to high sealing potential, indicating high clay content and strong sealing capability.

4.4. Discussion

This study conducts geostress calculations for the strata in the Zhuhai Formation of the Pearl River Estuary Basin and detailed the variations in stratigraphic density, these data reflect the complexity of the geological structure and the heterogeneity of the stress field, which is consistent with the studies of Zhuge et al. [24], providing a scientific basis for a more accurate assessment of fault sealing properties. Moreover, this result aligns with the findings of Yao et al., who investigated fault sealing and fluid pressurization processes during seismic events. They emphasized the dynamic characteristics of fault sealing under seismic conditions, which are consistent with the significant influence of the in- situ stress field on fault sealing. Similarly, Morgan et al. demonstrated that deformation caused by thrusting enhanced fault sealing, supporting the conclusion that the distribution and variation of in-situ stress were closely related to the physical and mechanical properties of the formation. These comparisons further underscore the importance of considering dynamic stress fields in fault sealing evaluations, particularly in tectonically active regions such as the Pearl River Mouth Basin.

In this study, the in-situ stress distribution of the Zhuhai Formation in the Pearl River Mouth Basin exhibited significant heterogeneity, primarily due to the complexity of the stratigraphic structure and the variability of fault activity. Variations in vertical stress, maximum principal stress, and minimum principal stress at different depths and regions reflect stress concentration and release phenomena within the formation. Stress concentration areas are often closely associated with fault zones or lithological transition zones, and the stress distribution in these areas can significantly influence fault sealing. For instance, stress concentration may lead to localized sliding or fracturing within fault zones, reducing sealing capacity, whereas stress release regions may enhance fault stability and improve sealing capacity. Additionally, stress heterogeneity may affect hydrocarbon migration and accumulation, with high- stress areas potentially forming effective sealing barriers and low-stress areas serving as migration pathways. This provides more reliable data support for fault sealing evaluations.

Compared to the study by Indhanu et al. [25], this study presents significant innovations in geostress calculation and fault sealing evaluation methods. Thus, by analyzing parameters such as stratigraphic density, stress distribution, Biot coefficient, and static Poisson's ratio at different depths, it provides rich foundational data and theoretical support.

5. Conclusions

This study systematically analyzed the in-situ stress distribution of the Zhuhai Formation in the Pearl River Mouth Basin and its impact on fault sealing using numerical simulation and dynamic-static parameter conversion methods. The findings indicate that the in-situ stress distribution within the Zhuhai Formation exhibits significant heterogeneity. Vertical stress, maximum principal stress, and minimum principal stress increase linearly with depth, ranging from 28.31 to 33.21 MPa, 36.64 to 43.68 MPa, and 30.32 to 35.61 MPa, respectively. The distribution of the stress field is closely associated with the physical and mechanical properties of the formation. Variations in formation density, Biot's coefficient, and static Poisson's ratio directly influence fault sealing performance. By employing a multi- factor comprehensive evaluation system, fault sealing capacity was classified into three levels: high, moderate, and low, providing scientific evidence and technical support for oil and gas exploration and development. The innovation of this study lies in integrating dynamic-static parameter conversion with numerical simulation techniques, proposing a more precise method for evaluating fault sealing. This approach addresses the limitations of traditional static parameter-based evaluations and provides a novel technical pathway and theoretical foundation for oil and gas exploration under complex geological conditions.

Despite the significant progress made in fault sealing evaluation, this study has several limitations. First, it primarily focuses on in-situ stress fields and rock mechanical parameters without sufficiently considering dynamic geological factors, such as seismic activity and geothermal flux, which may significantly affect fault sealing in tectonically active regions. Second, the data were mainly obtained from a limited number of wells in the Zhuhai Formation of the Pearl River Mouth Basin. While locally representative, broader regional applicability requires further validation. Additionally, the accuracy of the dynamic-static parameter conversion method depends on limited experimental data, necessitating further optimization through additional core experiments and field tests in the future. Nonetheless, the findings of this study hold significant scientific value and practical relevance. By improving data collection and processing methods, the precision and reliability of fault sealing evaluations can be further enhanced, providing robust technical support for the efficient exploration and development of oil and gas resources.

References

[1] J. Ding, S. Yu, Z. Liu, S. Wang, and J. Lu, "Fault diagnosis of dry gas seal operation status based on acoustic emission monitoring", *Lubricants*, vol. 12, no. 2, art. no. 35, 2024, doi: 10.3390/lubricants12020035.

[2] Q. Wang, et al., "Application of machine learning for evaluating and predicting fault seals: A case study in the Huimin depression, Bohai Bay Basin, Eastern China", *Geoenergy Science and Engineering*, vol. 228, art. no. 212064, 2023, doi: 10.1016/j.geoen.2023.212064.

[3] Q. Wang, Y. Song, H. Li, Y. Shu, and Y. Xiao, "Tribological behavior characterization and Fault Detection of mechanical seals based on face vibration acceleration measurements", *Lubricants*, vol. 11, no. 10, art. no. 430, 2023, doi: 10.3390/lubricants11100430.

[4] Y. Li, et al., "Key issues in water sealing performance of underground oil storage caverns: Advances and perspectives", *Journal of Rock Mechanics and Geotechnical Engineering*, vol. 15, no. 10, pp. 2787–2802, 2023, doi: 10.1016/j.jrmge.2022.12.017.

[5] C. Wang, C. Yin, X. Shi, D. Zhang, M. Liao, and R. Zhang, "Research on geophysical response analysis and prediction technology of geostress in the shale gas area of the southern Sichuan Basin", *Frontiers in Energy Research*, vol. 11, art. no. 1328236, 2024, doi: 10.3389/fenrg.2023.1328236.

[6] W. Cai, H. Zhu, W. Liang, B.T. Vu, and W. Wu, "Physical and numerical investigation on nonlinear mechanical properties of deep-buried rock tunnel excavation unloading under complicated ground stresses", *Tunnelling and Underground Space Technology*, vol. 138, art. no. 105197, 2023, doi: 10.1016/j.tust.2023.105197.

[7] L. Yao, S. Ma, and G. Di Toro, "Coseismic fault sealing and fluid pressurization during earthquakes", *Nature Communications*, vol. 14, art. no. 1136, 2023, doi: 10.1038/s41467-023-36839-9.

[8] J.K. Morgan, et al., "Seafloor overthrusting causes ductile fault deformation and fault sealing along the Northern Hikurangi Margin", *Earth and Planetary Science Letters*, vol. 593, art. no. 117651, 2022, 10.1016/j.epsl.2022.117651

[9] B. Yang, Q. Fu, J. Liu, W. Ma, and S. Zhao, "Study on fault sealing of the Lishui West Sag in the East China Sea Basin", *Frontiers in Earth Science*, vol. 10, art. no. 1012324, 2023, doi: 10.3389/feart.2022.1012324.

[10] Z. Esmaeilzadeh, D.W. Eaton, N. Hosseini, and D. Zeinabady, "Sealing faults and fluid-induced seismicity", *Philosophical Transactions A*, vol. 382, no. 2276, art. no. 20230418, 2024, doi: 10.1098/rsta.2023.0418.

[11] G. Zhang, et al., "Sealing capacity evaluation of underground gas storage under intricate geological conditions", *Energy Geoscience*, vol. 5, no. 3, art. no. 100292, 2024, doi: 10.1016/j.engeos.2024.100292.

[12] M. Congro, A.S. Zanatta, K. Nunes, R. Quevedo, B.R.B.M. Carvalho, and D. Roehl, "Determination of fault damage zones in sandstone rocks using numerical models and statistical analyses", *Geomechanics for Energy and the Environment*, vol. 36, art. no. 100495, 2023, doi: 10.1016/j.gete.2023.100495.

[13] Y. Zhao, et al., "A review of hydromechanical coupling tests, theoretical and numerical analyses in rock materials", *Water*, vol. 15, no. 13, art. no. 2309, 2023, doi: 10.3390/w15132309.

[14] C. Wu, X. Zhou, L. Wang, Z. Li, and X. Zhang, "Failure mechanism of full- length grouted bolts for large-deformation tunnels under high geo-stress: A case study", *Engineering Failure Analysis*, vol. 159, art. no. 108021, 2024, doi: 10.1016/j.engfailanal.2024.108021.

[15] L. Zhu, T. Huang, H. Li, Z. Zhou, and X. Liao, "Numerical study on the influence of fault structure on the geostress field", *Sustainability*, vol. 15, no. 18, art. no. 13734, 2023, doi: 10.3390/su151813734.

[16] F. Han, N. Jiang, Y. Yao, C. Zhou, and Y. Yang, "Dynamic response characteristics and instability mechanism of layered surrounding rock tunnels affected by geostress under dynamic and static loads", *Engineering Failure Analysis*, vol. 160, art. no. 108202, 2024, doi: 10.1016/j.engfailanal.2024.108202.

[17] Y. Zhang, K. Xu, H. Zhang, S. Lai, J. Liang, and Z. Qian, "Numerical simulation and application of ground stress field in ultra-deep strike-slip faults-taking the FI12 fault zone in the Fuman Oilfield as an example", *Frontiers in Energy Research*, vol. 12, art. no. 1361247, 2024, doi: 10.3389/fenrg.2024.1361247.

[18] Z. Han, M. Li, C. Wang, J. Wang, and X. Huang, "Application and discussion of the borehole radial deformation method in deep borehole geostress measurement", *Frontiers in Earth Science*, vol. 11, art. no. 1102276, 2023, doi: 10.3389/feart.2023.1102276.

[19] M. Lei, B. Zhu, C. Gong, W. Ding, and L. Liu, "Sealing performance of a precast tunnel gasketed joint under high hydrostatic pressures: Site investigation and detailed numerical modeling", *Tunnelling and Underground Space Technology*, vol. 115, art. no. 104082, 2021, doi: 10.1016/j.tust.2021.104082.

[20] X. Shi, P. Yang, L. Li, and F. Wu, "Investigating mechanical properties of cemented soil under static and dynamic loading after a freeze-thaw cycle", *KSCE Journal of Civil Engineering*, vol. 27, no. 3, pp. 978–991, 2023, doi: 10.1007/s12205-023-0209-7.

[21] Z. Tang, Z. Wu, D. Jia, and J. Lv, "The distribution law of ground stress field in Yingcheng coal mine based on rhino surface modeling", *Processes*, vol. 12, no. 4, art. no. 668, 2024, doi: 10.3390/pr12040668.

[22] M. Superczyńska, M. Maślakowski, and R. Mieszkowski, "Three-dimensional interpretation of geophysical and geotechnical investigation of landslides", *Archives of Civil Engineering*, vol. 70, no. 4, pp. 99–111, 2024, doi: 10.24425/ace.2024.151882.

[23] S. Ban, et al., "The application of the fuzzy comprehensive evaluation method in the sealing evaluation of caprocks in underground gas storage", *Applied Sciences*, vol. 13, no. 17, art. no. 9753, 2023, doi: 10.3390/app13179753.

[24] X. Zhuge, J. Hong, C. Wang, J. Wang, and H. Xia, "Dynamic evaluation of sealing and site optimization for underground gas storage in depleted gas reserve: A case study", *Applied Sciences*, vol. 14, no. 1, art. no. 298, 2023, doi: 10.3390/app14010298.

[25] T. Indhanu, W. Srisakul, T. Chompoorat, and T. Chub-uppakarn, "Evaluation and mitigation of ground loss and shear failure in silty sand due to static liquefaction potential with geotextile filtration", *International Journal of Geosynthetics and Ground Engineering*, vol. 9, no. 6, art. no. 80, 2023, doi: 10.1007/s40891-023-00496-1.

Received: 2024-09-19, Revised: 2025-04-29